Acta Materialia 245 (2023) 118640

Contents lists available at ScienceDirect

Acta Materialia

journal homepage: www.elsevier.com/locate/actamat

Giant flexoelectric coefficients at critical ferroelectric transition

Xiaoqin Ke [a,#,*], Zhengkai Hong [a,#], Qianqian Ma [b,#], Xin Wen [b], Zhiguo Wang [c], Sen Yang [a,*], Lixue Zhang [a], Dong Wang [a], Longlong Shu [c], Qian Deng [d,e,*], Shengping Shen [b], Xiaobing Ren [a,f], Yunzhi Wang [g]

[a] School of Physics, MOE Key Laboratory for Nonequilibrium Synthesis and Modulation of Condensed Matter, Frontier Institute of Science and Technology, State Key Laboratory for Mechanical Behavior of Materials, Xi'an Jiaotong University, Xi'an 710049, China
[b] State Key Laboratory for Strength and Vibration of Mechanical Structures, School of Aerospace Engineering, Xi'an Jiaotong University, Xi'an 710049, China
[c] School of Materials Science and Engineering, Nanchang University, Nanchang 330031, China
[d] School of Aerospace Engineering, Huazhong University of Science and Technology, Wuhan, 430074, China
[e] Hubei Key Laboratory of Engineering Structural Analysis and Safety Assessment, Wuhan, 430074, China
[f] National Institute for Materials Science, Tsukuba 305-0047, Japan
[g] Department of Materials Science and Engineering, The Ohio State University, Columbus, OH 43210, United States

A B S T R A C T

Flexoelectric materials, which could generate polarization in response to a strain gradient, could be utilized in a wide range of devices such as actuators and sensors. However, the flexoelectric coefficients of most dielectrics are too small to be utilized. One of the most promising flexoelectric materials is ferroelectrics whose flexoelectric coefficients are orders of magnitude higher than those of ordinary dielectrics. Despite of intensive research in the past twenty years, the record-high flexoelectric coefficient (μ_{1122}=100μC/m) of $Ba_{0.67}Sr_{0.33}TiO_3$ ferroelectric has not been surpassed. Here we show that by tuning the first-order paraelectric-ferroelectric phase transition of $BaTiO_3$ to near-critical through doping $BaZrO_3$, a drastic enhancement of flexoelectric coefficient (μ_{1122}=140μC/m) occurs, which is ascribed to the enhancement of both intrinsic and extrinsic flexoelectricity resulting from the strong lattice instability at the critical transition. This study demonstrates a general design method to achieve high flexoelectric coefficients in a wide range of ferroelectric systems through searching for critical ferroelectric transition points.

1. Introduction

Upon the application of a non-uniform deformation such as a strain gradient, a dielectric material that may not necessarily be piezoelectric would get polarized due to the flexoelectric effect [1, 2]. Mathematically, flexoelectricity in dielectric solids is expressed by

$$P_i = \mu_{ijkl}\frac{\partial e_{jk}}{\partial x_l} \quad (1)$$

where P_i denotes polarization induced by the flexoelectric effect, e_{jk} is the strain, and the fourth order tensor μ_{ijkl} is the flexoelectric coefficient which links polarization and strain gradient in a dielectric material. Since the strain gradient in a sample scales up when its size decreases, the flexoelectric effect is expected to be much stronger at the nanoscale [3]. Thus, recently, various novel applications of flexoelectricity at the nanoscale have been proposed [4,5]. Moreover, since flexoelectricity directly couples polarization and strain gradient, it provides various possibilities for designing novel devices [6,7]. For example, the polarization and curvature of a cantilever beam can be directly coupled by the flexoelectric effect, which motivates the ideas of flexoelectric energy harvesting (an electrical output induced by bending a cantilever beam) [8] and flexoelectric actuating (bending of a cantilever beam upon the application of a uniform electric field across its thickness) [9]. Another example is to directly measure a strain gradient using a flexoelectric sensor [10]. In addition, flexoelectricity has also been employed to explain the charge transfer driver for the triboelectricity effect [11], the formation of chiral domain wall in ferroelectrics [12,13], as well as some important biological phenomena such as self-healing of bones [14] and the working mechanism of cochlea [15].

However, the flexoelectric effect observed for most dielectrics is rather small even at the nanoscale because the flexoelectric coefficients, μ_{ijkl}, for most dielectric ceramics such as NaCl are extremely low (0.01nC/m~1nC/m) [1,16–18]. Since the flexoelectric coefficient scales with dielectric permittivity [19,20], large flexoelectric coefficients

* Corresponding authors.
E-mail addresses: kexiaoqin@xjtu.edu.cn (X. Ke), yangsen@mail.xjtu.edu.cn (S. Yang), tonydqian@hust.edu.cn (Q. Deng).
# These authors contribute equally to this work.

https://doi.org/10.1016/j.actamat.2022.118640
Received 18 March 2022; Received in revised form 22 November 2022; Accepted 19 December 2022
Available online 20 December 2022

could occur near the Curie temperature of ferroelectric materials due to the large dielectric permittivity at paraelectric-ferroelectric transition and it has been found that ferroelectric materials can exhibit several orders of magnitude higher flexoelectric coefficients (1∼100μC/m) than those of ordinary dielectrics [21–27]. However, the flexoelectric coefficients of ferroelectric materials are still not comparable with the piezoelectric coefficients and require further enhancement for practical applications [28,29]. More recent efforts have been focusing on how to enhance the apparent flexoelectric coefficients of ferroelectric materials by designing various microstructures [30–32] or intentionally introducing different kinds of flexoelectric-like effect [33–37]. Nevertheless, how to further increase the conventional flexoelectric coefficients of pure ferroelectric materials is still a difficulty challenge.

Among the various ferroelectric ceramics studied such as $Ba_{1-x}Sr_xTiO_3$ [21], $BaTiO_3$-$Bi(Zn_{1/2}Ti_{1/2})O_3$ [38], $PbMg_{1/3}Nb_{2/3}O_3$ [22], $PbZr_xTi_{1-x}O_3$ [23,26], $Pb_{1-x}Sr_xTiO_3$ [24], $BaTiO_3$ [25], and $BaTi_{1-x}Sn_xO_3$ [27], $PbMg_{1/3}Nb_{2/3}O_3$-$PbTiO_3$ [39], $Ba_{0.67}Sr_{0.33}TiO_3$ exhibits the largest flexoelectric μ_{1122} coefficient (100μC/m) at T_C and has become the "flagship" flexoelectric materials [30,40,41]. Although the large flexoelectric coefficient of $Ba_{0.67}Sr_{0.33}TiO_3$ is related to the large dielectric permittivity at its T_C [19,20], the large permittivity alone cannot explain the result because other ferroelectric ceramics such as $PbMg_{1/3}Nb_{2/3}O_3$ exhibit a similar magnitude of the dielectric permittivity but a much lower μ_{1122} flexoelectric coefficient [22]. Despite of extensive research on the mechanisms of the high flexoelectric coefficient in $Ba_{0.67}Sr_{0.33}TiO_3$, as well as on searching for ferroelectric materials with higher flexoelectric coefficients in the past twenty years [19,27,40–43], the flexoelectric coefficient of $Ba_{0.67}Sr_{0.33}TiO_3$ has not been surpassed.

Here in this work we substitute "Ti" with "Zr" in $BaTiO_3$ and obtain ceramic samples of different $BaTi_{1-x}Zr_xO_3$ (abbreviated as BT-*x*Zr hereafter) solid solutions ($x = 0$, 0.04, 0.08, 0.11, 0.12, 0.13, 0.15, 0.18). It is demonstrated that a giant flexoelectric coefficient (140μC/m) occurs at BT-0.12Zr which exhibits a near-critical ferroelectric transition due to the convergence of four phases (cubic, tetragonal, orthorhombic and rhombohedral) in the phase diagram. Such giant flexoelectric coefficient is ∼1.4 times that of the former flagship flexoelectric materials $BaSr_{0.33}Ti_{0.67}O_3$, and ∼3.5 times that of undoped $BaTiO_3$. Further study shows that the giant flexoelectric coefficient achieved at BT-0.12Zr ceramic could originate from the enhancement of both the intrinsic and a particular extrinsic flexoelectric responses as a result of the strong lattice instability at the critical ferroelectric transition.

2. Experimental methods

Ceramic disks of $BaTi_{1-x}Zr_xO_3$ solid solutions ($x = 0$, 0.04, 0.08, 0.11, 0.12, 0.13, 0.15, 0.18) were obtained by the conventional solid-state reaction method. Raw powders of $BaCO_3$, TiO_2, $BaZrO_3$ with high purity (>99.9) were weighed and ball milled using zirconium balls for 10 h in polyethylene jars with ethanol as media. After drying, the mixture was calcined at 1300°C for 3 h. The calcined powders were ball milled again for 6 h. After drying, the powders were mixed with 5 wt% PVA solution and uniaxially pressed into small and big disks. The diameter of the small disks is 1 cm and the thickness is 1 mm. The diameter of the big disks is 20 mm and the thickness is 1 mm. The green disks were finally sintered at 1475 °C for 3 h.

For dielectric and hysteresis loop measurements, the disks were coated with silver paste on both sides. The temperature dependent dielectric permittivity was measured by an LCR meter (3532–50 LCR, HIOKI) in the Delta chamber. The hysteresis loop was measured using a Radiant precision workstation (Trek model 609A, USA). The heat flow curve was measured by a differential scanning calorimeter (DSC, TA Instruments Q200) at a heating rate of 10°C/min, and the latent heat was calculated from the corresponding heat flow peak. The grain structures of the samples were observed by optical microscopy.

The flexoelectric coefficient was measured using the three-point-bending method [17,35,44,45]. The ceramics disks were cut to beams (3 mm wide, 15 mm long, and 1 mm thick) using a diamond-wire cutting machine (STX-1202, MTI). Pt electrodes of area (A) 15mm^2 were deposited on its upper and lower surfaces by sputtering. Copper wires were attached to the electrodes with silver paste. The experimental setup for the flexoelectric measurement is given (See Supplementary Fig. S1). A load machine (electroforce 3230, TA) was used to apply a sinusoidal oscillatory force with a frequency of 1 Hz on the center (Line AB) of the beam's upper surface. Two supporting edges were separated by $L = 10$ mm. A charge amplifier (2692, BK) and an oscilloscope (MDO3104, Tektronix) were used to detect the polarization charges Q, which can be converted to average polarization $\overline{P}$ through $\overline{P} = Q/A$. Since the charge amplifier is only sensitive to AC signals, the polarization charges caused by the static force can be automatically screened out in our experiment. The optical gratings in the load machine were used to measure the displacement of the sample center δ. The average strain gradient across the thickness direction was obtained according to the formula proposed in [17]: $\overline{\frac{\partial \varepsilon_{11}}{\partial x_2}} = \frac{12\delta}{L^3}(L-a)$, where a is the half-length of the electrodes. The effective flexoelectric coefficient could then be calculated by: $\mu_{1122}^{eff} = \overline{P}/\overline{\frac{\partial \varepsilon_{11}}{\partial x_2}}$. To eliminate electromagnetic interferences from the environment, we filtered the data and extracted the signal at 1 Hz. For temperature dependent measurements, a resistive heater was used to control the temperature and the heating rate was set to be 1°C /min. The flexoelectric coefficient was measured 3 times for each sample.

Note that there are two other methods (i.e., the cantilever-beam method [22–24,26] and the four-point-bending method [27]) commonly used to measure the transverse flexoelectric coefficient of dielectric solids. The experimental setups for the three methods are compared in the supplementary materials (See Supplementary Fig. S2). All three methods have been successfully employed to measure the transverse flexoelectric coefficient of ferroelectric materials and each of them has its own pros and cons. For example, the experimental setup for the CB method is relatively simple while the setups for the TP and FP methods are more complex. On the other hand, the CP method can only measure the flexoelectric coefficient at small strain gradient, while the FP and TP methods can measure the flexoelectric coefficient at relatively large strain gradient. In this work, we employed the TP method to measure the transverse flexoelectric coefficient of our ceramic samples because of our easy access to the TP setup.

3. Results and discussions

3.1. Giant flexoelectric coefficient obtained at BT-0.12Zr ceramic

All BT-*x*Zr ceramic samples are single-phase as inferred from their room-temperature XRD profiles (See Supplementary Fig. S3) and they are insulating as can be inferred from their polarization-electric field loops at room temperature (See Supplementary Fig. S4).

The transverse flexoelectric coefficient (μ_{1122}) of four representative compositions (BT-0.08Zr, BT-0.11Zr, BT-0.12Zr, and BT-0.15Zr) are then measured. It has been observed that the room-temperature polarization of all four samples exhibits a nearly linear relationship with the strain gradient (See Supplementary Fig. S5), which indicates negligible contributions from domain wall motion or flexoelectric poling. Fig. 1(a) plots the variation of the flexoelectric coefficient (μ_{1122}) with temperature for these four representative compositions. Consistent with the previous reports [22–28], all compositions display a peak value of the flexoelectric coefficient near their T_C. More importantly, it can be shown that BT-0.12Zr exhibits the largest flexoelectric coefficient (140μC/m) near its T_C as compared to the nearby compositions. The high flexoelectric μ_{1122} coefficient (140μC/m) of BT-0.12Zr is not only the largest value in the BT-*x*Zr system, but is also much larger than that of the "flagship" flexoelectric material $Ba_{0.67}Sr_{0.33}TiO_3$ (100μC/m). Fig. 1(b) compares the flexoelectric μ_{1122} coefficient of our BT-0.12Zr sample near T_C with that of other compositions in BT-*x*Zr system as well as that

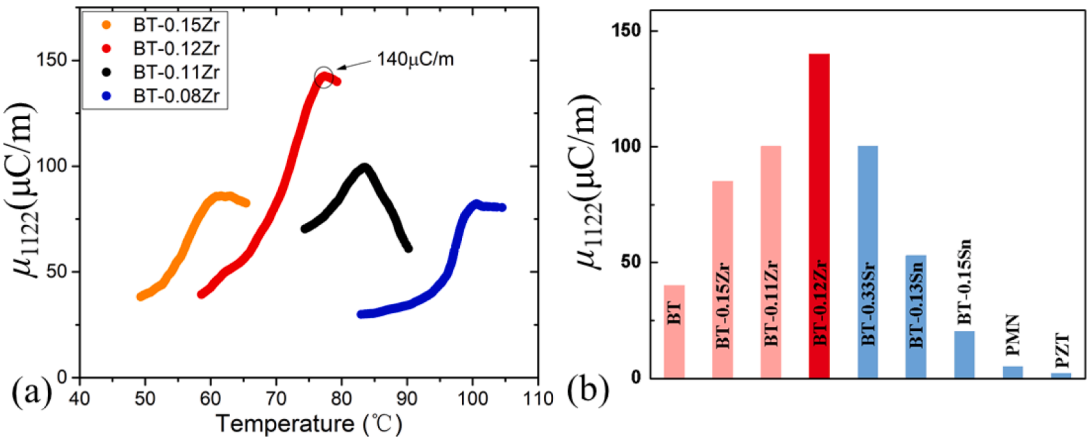

Fig. 1. (a) Variation of the flexoelectric coefficient (μ_{1122}) with temperature for BT-0.08Zr, BT-0.11Zr, BT-0.12Zr, and BT-0.15Zr. (b) Comparison of the flexoelectric coefficient μ_{1122} of BT-0.12Zr at its T_C with other ferroelectric ceramics [22–28].

of other ferroelectric ceramics studied in literature obtained by similar fabrication method [22–28]. Note that by changing the heat treatment history of the sample, the flexoelectric coefficient could even be further elevated for BT-0.12Zr [37]. It can be readily seen from Fig. 1(b) that the obtained high μ_{1122} flexoelectric coefficient (140μC/m) of BT-0.12Zr is ~3.5 times of that of undoped $BaTiO_3$ ceramic (~40μC/m) and ~1.4 times of that of BT-0.11Zr as well as the former "flagship" flexoelectric material $Ba_{0.67}Sr_{0.33}TiO_3$ (100μC/m).

3.2. The relationship between the flexoelectric coefficient at t_c of BT-xZr ceramics and the order of their ferroelectric phase transition

To explore the reason why BT-0.12Zr exhibits such a high flexoelectric coefficient, the partial phase diagram of the BT-*x*Zr system determined from the dielectric permittivity spectrum of the studied compositions (See Supplementary Fig. S6) and the characteristic X-ray diffraction results of three representative compositions (See Supplementary Fig. S7) is plotted in Fig. 2(a). The obtained phase diagram is consistent with previous results [46,47]. It is readily seen in the phase diagram that the cubic (C,$Pm\bar{3}m$), tetragonal (T, *P4mm*), orthorhombic (O, *Amm2*) and rhombohedral (R, *R3m*) phases of BT converge at a quadruple point (composition BT-0.12Zr), which is the composition exhibiting the highest flexoelectric μ_{1122} coefficient as illustrated in Fig. 1(a). Fig. 2(b) plots the values of thermal transition hysteresis of C-T, C-R, T-O and O-R transitions at all compositions. The thermal hysteresis was measured by the difference of the phase transition temperature upon heating and cooling as illustrated in the inset of Fig. 2(b). The results demonstrate that the thermal hysteresis values of all four transitions (C-T, C-R, T-O and O-R) become the smallest and approach zero as the composition approaches the quadruple point (BT-0.12Zr) from both $x<0.12$ and $x>0.12$ sides, which thus indicate a *near-critical* nature of the paraelectric-ferroelectric transition at the quadruple point and is consistent with our previous theoretical predictions [48]. In addition, the latent heat calculated from the heat flow curves of different compositions in BT-*x*Zr system also supports the near-critical nature of the paraelectric-ferroelectric transition of BT-0.12Zr (See Supplementary Fig. S8). Therefore, the high flexoelectric coefficient obtained at BT-0.12Zr could be associated with the near-critical nature of the paraelectric-ferroelectric transition at the C-T-O-R quadruple point.

To verify this, Fig. 3 then plots the variation of flexoelectric μ_{1122} coefficient at T_C of BT-*x*Zr ceramics with the thermal hysteresis of their paraelectric-ferroelectric transition. It is illustrated that the flexoelectric μ_{1122} coefficient of BT-*x*Zr monotonically increases with the decrease of transition thermal hysteresis and reaches the largest value (140μC/m) at BT-0.12Zr as the thermal hysteresis of BT-0.12Zr approaches zero. Therefore, it is clear that the dramatic enhancement of flexoelectric coefficient of BT-0.12Zr is indeed associated with the near-critical paraelectric-ferroelectric transition of it.

3.3. Origin of the giant flexoelectric coefficient at critical ferroelectric transition

The flexoelectric coefficients of ferroelectric ceramics depends on both the intrinsic flexoelectricity and the possible extrinsic effects [40].

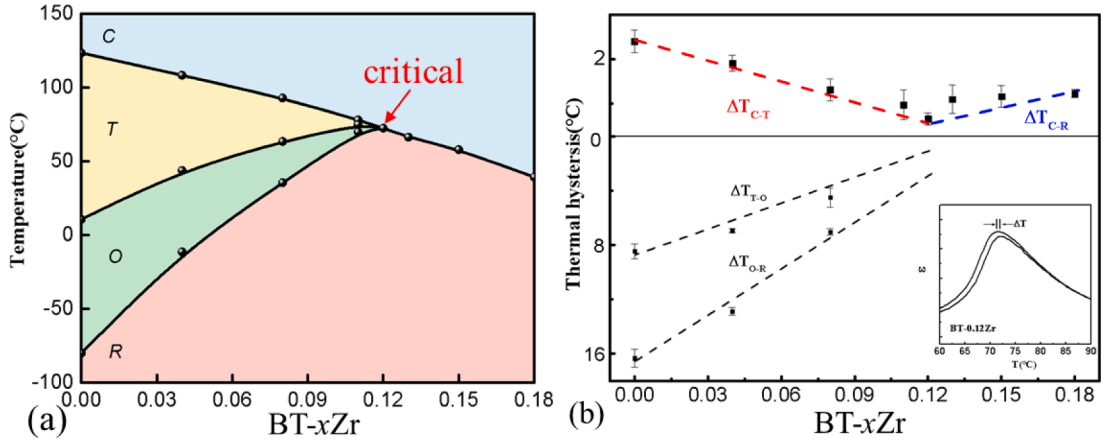

Fig. 2. (a) Partial phase diagram of BT-xZr system; (b) Thermal hysteresis of C-T, C-R, T-O and O-R transition of different BT-*x*Zr compositions. ΔT_{C-T}, ΔT_{C-R},ΔT_{T-O}, and ΔT_{O-R} are the thermal hysteresis of C-T, C-R, T-O and O-R transitions, respectively.

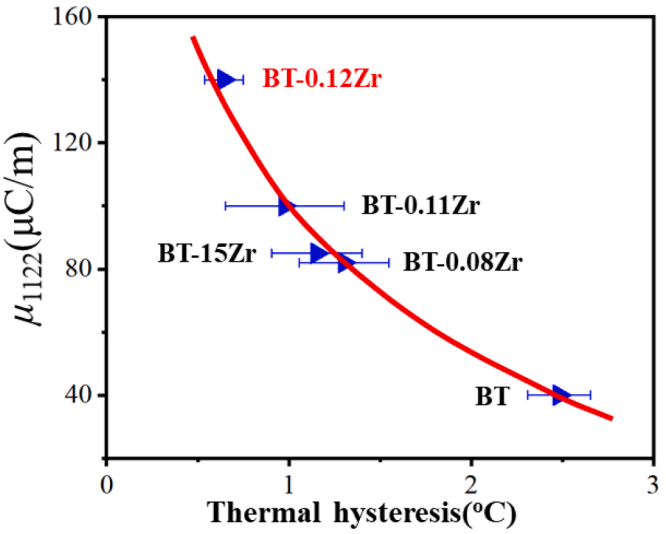

Fig. 3. Variation of flexoelectric μ_{1122} coefficient at T_C with the thermal hysteresis of paraelectric-ferroelectric transition for BT-*x*Zr ceramics.

Below we will explore the origin of the giant flexoelectric coefficient at the critical ferroelectric transition from the aspects of both the intrinsic effect and extrinsic effect.

3.3.1. *Enhanced intrinsic flexoelectric coefficient at critical ferroelectric transition*

To understand the mechanisms underlying the high flexoelectric coefficient at the critical ferroelectric transition, we first analyze the intrinsic flexoelectricity at the paraelectric-ferroelectric transition using one-dimensional (1D) Landau-Ginzburg-Devonshire theory shown below (More advanced models such as the phase field model [12,13,49] shall be developed in the future for stricter and more concrete interpretations). The Landau free energy of a ferroelectric system at a stress-free state can be approximated by a 6th order landau polynomial [48]:

$$f = \alpha_0(T - T_0)P^2 + \beta P^4 + \gamma P^6 \quad (2)$$

where α_0, β, and γ are the dielectric stiffness coefficients, P is the magnitude of polarization, T is temperature, and T_0 is the Curie-Weiss temperature. The black curves in Fig. 4(a)-(c) schematically show three different cases: a) a typical first-order ferroelectric transition ($\beta=\beta_0$, $\beta_0<0$), b) a weaker first-order transition ($\beta=0.75\beta_0$), and c) a critical transition ($\beta=0$). For these three cases, α_0, γ and T_0 are kept constant while T gradually decreases from a value larger than T_0 to T_0 in order to reach the thermodynamic equilibrium between the paraelectric and ferroelectric phases at T_C (See Supplementary Table S1). From Figs. 4(a) to 4(c) it is readily seen that from the relatively strong first-order to a weaker first-order and finally to a critical ferroelectric transition, the energy barrier between the paraelectric and ferroelectric phases becomes smaller and smaller, and finally vanishes. Correspondingly, the transition thermal hysteresis would be gradually reduced to zero and the curvature of the free energy curve at $P = 0$ also gradually decreases to near zero. Under a finite strain gradient field, a coupling term relating strain gradient and polarization ($-f_0\frac{\partial e}{\partial x}P$, where $\frac{\partial e}{\partial x}$ is the strain gradient, f_0 is the flexocoupling coefficient) should enter the total Landau free energy of a ferroelectric system, which changes the free energy into (here the homogeneous strain field is neglected for simplicity and it would not qualitatively change the results [20,50,51])

$$f = \alpha_0(T - T_0)P^2 + \beta P^4 + \gamma P^6 - f_0\frac{\partial e}{\partial x}P \quad (3)$$

The last coupling term in Eq. (3) (denoted by the dotted gray lines in Fig. 4(a)-(c)) would skew the free energy curves at all three cases plotted according to Eq. (2) (black curves) and turn them into the red curves. Comparing the free energy curves under zero external field (ZF) with that under a finite strain gradient field (UF) in Fig. 4(a)-(c), it is readily seen that the initial paraelectric phase with $P = 0$ (denoted by the black dots) under zero strain gradient field moves to a new equilibrium polarization state ($P\neq0$, denoted by the red dots) under the strain gradient field. Such polarization change (ΔP) from zero P to a finite P is thus induced by the strain gradient field and is flexoelectricity by definition. As demonstrated in Fig. 4(a)-(c), ΔP increases as the first-order ferroelectric transition ($\beta=\beta_0$) becomes weaker ($\beta=0.75\beta_0$) and then drastically increases as the ferroelectric transition becomes critical ($\beta=0$). Therefore, it is clear that the nearly vanishing energy barrier between the paraelectric and ferroelectric phases and thus easy distortion of the paraelectric phase structure by external strain gradient field lead to the dramatic enhancement of the intrinsic flexoelectric coefficient and thus contribute to the giant flexoelectric coefficient obtained at the near-critical ferroelectric transition of BT-0.12Zr ceramic.

3.3.2. *Enhanced extrinsic flexoelectricity at critical ferroelectric transition*

The above theoretical analysis based on the Landau theory clearly demonstrates the physical origin of the much-enhanced intrinsic flexoelectricity at critical ferroelectric transitions. However, there is a remaining challenging question why a large discrepancy exists between the experimentally measured flexocoupling coefficients and the theoretically predicted intrinsic one. Fig. 5 plots the experimentally measured flexocoupling coefficients at the T_C of all four BT-*x*Zr ceramics. It is illustrated that the flexocoupling coefficients at T_C of all four compositions (>270 V) are one to two orders of magnitude larger than

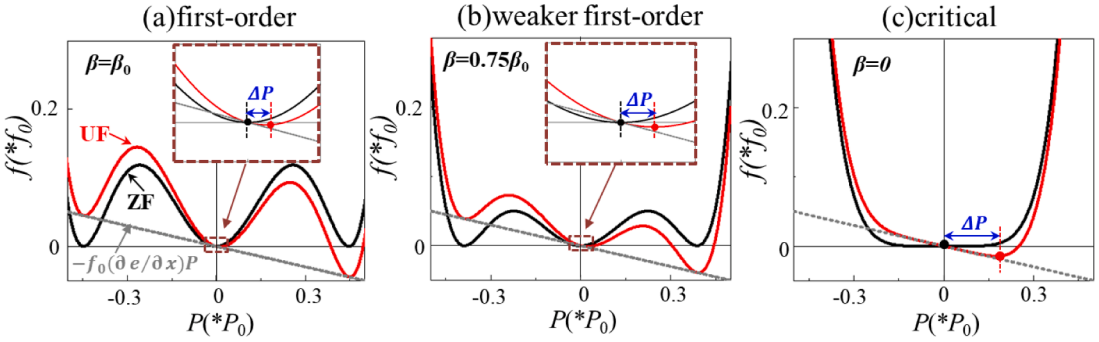

Fig. 4. Schematic of the Landau free energy curves at T_C under zero external field (abbreviated as ZF, black curves) and under a finite strain gradient field (abbreviated as UF, red curves) for (a) a first-order ferroelectric transition($\beta=\beta_0$), (b) a weak first-order ferroelectric transition($\beta=0.75\beta_0$), and (c) a critical ferroelectric transition($\beta=0$). The dotted gray lines represent the coupling term ($-f_0(\partial e/\partial x)P$). The black dots denote the initial polarization and the red dots denotes the new equilibrium polarization of the paraelectric phase under strain gradient for each case. The difference between the polarization at the red dot and that at the black dot (ΔP) at each case is the polarization change induced by the strain gradient field (intrinsic flexoelectricity).

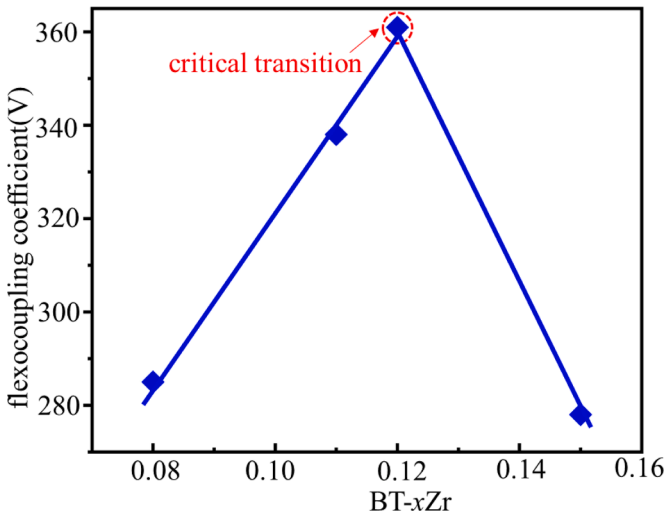

Fig. 5. The measured flexocoupling coefficient at T_C of the BT-*x*Zr ceramics.

the theoretically predicted intrinsic one (1–10 V) [51], which thus indicates that the measured flexoelectric coefficients of BT-*x*Zr ceramics should also include much extrinsic contribution [44,45,52]. Furthermore, it is seen from Fig. 5 that BT-0.12Zr exhibits the largest flexocoupling coefficients (~360 V) as compared to nearby off-critical compositions, suggesting that the critical ferroelectric transition not only maximizes the intrinsic flexoelectric effect discussed above, but also maximizes at least one of those extrinsic effects proposed in the literature[43–45,53].

The extrinsic mechanisms such as the barrier-layer mechanism [34] and the grain boundary effect [44] play a minor role here because our ceramic samples are all insulating (See Supplementary Fig. S4) and the grains in all the samples are similar in size (See Supplementary Fig. S9). In addition, all unpoled samples exhibit a piezoelectric d_{33} coefficient of zero both above and below their Curie temperatures, indicating negligible contribution from residual polarization. The possible extrinsic mechanism that matters here could be the flexoelectric-like effect caused by the asymmetric distribution of piezoelectric coefficients across the sample [28]. It is illustrated by Abdollahi et al. that the piezoelectric coefficient variation across the sample could lead to a large flexoelectric-like effect which scales with the gradient of the piezoelectric coefficient [28]. The critical ferroelectric transition is shown theoretically to exhibit infinitely large piezoelectric coefficient at T_C due to the strong lattice instability (as illustrated in Fig. 4(c)) [48], which has been experimentally verified by the largest piezoelectric coefficient obtained at T_C of BT-0.12Zr in $BaZr_xTi_{1-x}O_3$ system [See Supplementary Fig. 10]. If the degree of local composition variation in all four samples (x = 0.08, 0.11, 0.12, 0.15) is similar, then the gradient of the piezoelectric coefficient across the sample should be the largest for the critical composition BT-0.12Zr as compared to those for the off-critical compositions, which thus could lead to the highest extrinsic flexoelectric effect at BT-0.12Zr.

It has been proposed in reference [28] that beam-bending experiments with different sample thickness can be performed to verify the contribution from the asymmetric piezoelectricity because the measured flexoelectric coefficient would decrease with thickness if the piezoelectricity distribution along the thickness direction is linear. However, in our samples the piezoelectric coefficient distribution along the thickness direction is random due to the random distribution of local compositions [53], therefore, although the piezoelectricity asymmetry would contribute to the flexoelectricity, there is no fixed relationship between the flexoelectric coefficient and sample thickness, which has been verified by our experimental results (See Supplementary Fig. S11).

Therefore, the giant flexoelectric coefficient obtained at the near-critical ferroelectric transition of BT-0.12Zr could be attributed to the enhancement of both the intrinsic and extrinsic flexoelectric response at the critical ferroelectric transition as a result of the strong lattice instability.

3.3.3. *Comparison with relaxor-$PbTiO_3$ system*

Based on the above analysis of the flexoelectric response of BT-0.12Zr, large dielectric permittivity and high piezoelectric coefficient can be two important factors leading to giant flexoelectric coefficient. One would note that relaxor-$PbTiO_3$ such as PMN-PT samples simultaneously possess large dielectric permittivity [44] and ultrahigh piezoelectric coefficient (d_{33}>2000pC/N) [54] but do not show giant flexoelectric coefficient as BT-0.12Zr does [44], which seems to contradict with our conclusions. However, the ultrahigh piezoelectric coefficient of PMN-PT is obtained at their single-crystal forms [54]. Their ceramic forms typically show piezoelectric d_{33} coefficients of ~700pC/N [55], which are at a similar level with that of BT-0.12Zr ceramics [Supplementary Fig. S10]. In addition, the piezoelectricity gradient in different systems might also be different. Thus, it is difficult to tell which composition, PMN-PT or BT-0.12Zr, would shows a larger extrinsic flexoelectric coefficient from the inhomogeneous distribution of piezoelectric coefficients. On the other hand, although both PMN-PT and BT-0.12Zr show large dielectric permittivity, the exact values of flexcoupling coefficients for the two systems are not known, making the direct comparison between the intrinsic flexoelectric coefficients of PMN-PT and BT-0.12Zr impractical.

3.4. *Implications of the giant flexoelectric coefficient at BT-0.12Zr*

The above results indicate that there is nothing special about "$Ba_{1-x}Sr_xTiO_3$" because $BaTi_{1-x}Zr_xO_3$ can exhibit a much larger flexoelectric coefficient, as long as the first-order ferroelectric transition of $BaTiO_3$ is effectively tuned to a near-critical transition by doping. We note that the former "flagship" flexoelectric material $Ba_{0.67}Sr_{0.33}TiO_3$ was reported to exhibit a weak first-order ferroelectric transition [21], which thus could help explain the origin of its high flexoelectric coefficient based on this work. Therefore, this work provides a general guidance for the design of functional ferroelectric ceramics with large flexoelectricity, i.e., through searching for the critical point in a given ferroelectric phase diagram. We expect that high flexoelectricity could also be found at the C-T-O-R quadruple points in other $BaTiO_3$-based ferroelectric systems such as $BaTi_{1-x}Hf_xO_3$ [56] because it demonstrates a similar phase diagram topology as that shown in Fig. 2(a) and, thus, should exhibit a critical ferroelectric transition at their quadruple points according to previous theory [48].

It has been obtained that the dielectric loss is small (<0.1%) for BT-0.12Zr (Supplementary Fig. 12) and the flexoelectric coefficient of BT-0.12Zr is weakly frequency dependent (Supplementary Fig. 13), both of which are helpful for practical applications of the giant flexoelectric coefficient at critical ferroelectric transition. On the other hand, the current high flexoelectric coefficient μ_{1122} of 140μC/m is obtained at a temperature (>70°C) much higher than room temperature. At room temperature the μ_{1122} of BT-0.12Zr has decreased to a value less than 10μC/m (Supplementary Fig. 5), which could limit the practical applications of BT-0.12Zr on flexoelectric devices. Nevertheless, this work could provide a way to design ferroelectric materials with high flexoelectric coefficients at room temperature, i.e., finding ferroelectric materials with critical ferroelectric transitions at room temperature.

4. Conclusions

In summary, we have achieved the highest flexoelectric coefficient μ_{1122} of 140μC/m by tuning the first-order paraelectric-ferroelectric transition of $BaTiO_3$ to near-critical through doping "Zr" (BT-0.12Zr). The flexoelectric coefficient of BT-0.12Zr is ~1.4 times of that of the former flagship flexoelectric materials $Ba_{0.67}Sr_{0.33}TiO_3$. The critical

ferroelectric transition exhibits a large flexoelectric coefficient because both the intrinsic and extrinsic flexoelectric responses could be maximized as a result of the strong lattice instability. The intrinsic flexoelectric coefficient is enhanced at the critical ferroelectric transition because the strong lattice instability leads to easy lattice distortion under an external strain gradient field. On the other hand, the extrinsic flexoelectric coefficient could be enhanced at the critical ferroelectric transition because the strong lattice instability leads to the highest piezoelectric coefficient, which in turn could lead to the largest gradient of piezoelectric coefficient across the sample and thus to the highest flexoelectric-like response. Our work indicates that finding the critical or near-critical paraelectric-ferroelectric phase transition is essential to achieve large flexoelectric coefficient in ferroelectric materials. This work could stimulate further experimental work on developing new ferroelectric materials with high flexoelectricity for practical applications by systematical search for critical ferroelectric transitions through high throughput first-principle calculations assisted by machine learning [57,58].

Declaration of Competing Interest

The authors declare that they have no known competing financial interests or personal relationships that could have appeared to influence the work reported in this paper.

Acknowledgements

XK, SY and QD acknowledge the support from the National Key R & D Program of China (2017YFE0119800) and the National Natural Science Foundation of China (Grant No. 52171189, 51802249, No. 52171190, and No. 91963111), Key Scientific and Technological Innovation Team of Shaanxi province (2020TD-001), Innovation Capability Support Program of Shaanxi (No. 2018PT-28, 2017KTPT-04), the Fundamental Research Funds for the Central Universities (China), the World-Class Universities (Disciplines), the Characteristic Development Guidance Funds for the Central Universities. YW acknowledges the US Natural Science Foundation under Grant No. DMR-1923929.

Supplementary materials

Supplementary material associated with this article can be found, in the online version, at doi:10.1016/j.actamat.2022.118640.

References

[1] P. Zubko, G. Catalan, A.K Tagantsev, Flexoelectric effect in solids, Annu. Rev. Mater. Res. 43 (2013) 387–421.
[2] S. Krichen, P. Sharma, Flexoelectricity: a perspective on an unusual electromechanical coupling, J. Appl. Mech. 83 (3) (2016), 030801.
[3] M.S. Majdoub, P. Sharma, T Cagin, Enhanced size-dependent piezoelectricity and elasticity in nanostructures due to the flexoelectric effect, Phys. Rev. B 77 (2008), 125424.
[4] D. Lee, S.M. Yang, J.G. Yoon, T.W Noh, Flexoelectric rectification of charge transport in strain-graded dielectrics, Nano Lett. 12 (2012) 6436–6440.
[5] H. Lu, C.W. Bark, D.E. Ojos, J. Alcala, C.B. Eom, G. Catalan, A. Gruverman, Mechanical writing of ferroelectric polarization, Science 336 (6077) (2012) 59–61.
[6] X. Jiang, W. Huang, S. Zhang, Flexoelectric nano-generator: materials, structures and devices, Nano Energy 2 (2013) 1079.
[7] Q. Deng, S. Lv, Z. Li, K. Tan, X. Liang, S. Shen, The impact of flexoelectricity on materials, devices, and physics, J. Appl. Phys. 128 (2020), 080902.
[8] Q. Deng, M. Kammoun, A. Erturk, P. Sharma, Nanoscale flexoelectric energy harvesting, Int. J. Solids Struct. 51 (2014) 3218–3225.
[9] U.K. Bhaskar, N. Banerjee, A. Abdollahi, Z. Wang, D.G. Schlom, G. Rijnders, G Catalan, A flexoelectric microelectromechanical system on silicon, Nat. Nanotechnol. 11 (2015) 263–266.
[10] W. Huang, X. Yan, S.R. Kwon, S. Zhang, F.G. Yuan, X. Jiang, Flexoelectric strain gradient detection using $Ba_{0.64}Sr_{0.36}TiO_3$ for sensing, Appl. Phys. Lett. 101 (2012), 252903.
[11] C.A. Mizzi, A.Y.W. Lin, L.D. Marks, Does Flexoelectricity Drive Triboelectricity? Phys. Rev. Lett. 123 (2019), 116103.
[12] P.V. Yudin, A.K. Tagantsev, E.A. Eliseev, A.N. Morozovska, N. Setter, Bichiral structure of ferroelectric domain walls driven by flexoelectricity, Phys. Rev. B 86 (2012), 134102.
[13] Y. Gu, M. Li, A.N. Morozovska, Y. Wang, E.A. Eliseev, V. Gopalan, L.-.Q. Chen, Flexoelectricity and ferroelectric domain structures: phase-field modelling and DFT calculations, Phys. Rev. B 89 (2014), 174111.
[14] F. Vasquez-Sancho, A. Abdollahi, D. Damjanovic, G Catalan, Flexoelectricity in Bones, Adv. Mater. 30 (2018), 1705316.
[15] Q. Deng, F. Ahmadpoor, W.E. Brownell, P. Sharma, The collusion of flexoelectricity and Hopf-bifurcation in the hearing mechanism, J. Mech. Phys. Solids 130 (2019) 245–261.
[16] J. Hong, D. Vanderbilt, First-principles theory and calculation of flexoelectricity, Phys. Rev. B 88 (2013), 174107.
[17] P. Zubko, G. Catalan, A. Buckley, P.R.L. Welche, J.F. Scott, Strain-Gradient-Induced Polarization in $SrTiO_3$ Single Crystals, Phys. Rev. Lett. 99 (2007), 167601.
[18] F. Zhang, P. Lv, Y. Zhang, S. Huang, C.-M. Wong, H.-.M. Yau, X. Chen, Z. Wen, X. Jiang, C. Zeng, J. Hong, J.-.Y Dai, Modulating the electrical transport in the two-dimensional electron gas at $LaAlO_3/SrTiO_3$ heterostructures by interfacial flexoelectricity, Phys. Rev. Lett. 122 (2019), 257601.
[19] P.V. Yudin, A.K. Tagantsev, Fundamentals of flexoelectricity in solids, Nanotechnology 24 (2013), 432001.
[20] A.K. Tagantsev, Piezoelectricity and flexoelectricity in crystalline dielectrics, Phys. Rev. B 34 (1986) 5883.
[21] W. Ma, L.E. Cross, Flexoelectric polarization of barium strontium titanate in the paraelectric state, Appl. Phys. Lett. 81 (18) (2002) 3440.
[22] W. Ma, L.E. Cross, Large flexoelectric polarization in ceramic lead magnesium niobate, Appl. Phys. Lett. 79 (2001) 4420.
[23] W. Ma, L.E Cross, Strain-gradient-induced electric polarization in lead zirconate titanate ceramics, Appl. Phys. Lett. 82 (2003) 3293.
[24] L.E. Cross, Flexoelectric effects: charge separation in insulating solids subjected to elastic strain gradients, J. Mater. Sci. 41 (2006) 53.
[25] W. Ma, L.E. Cross, Flexoelectricity of barium titanate, Appl. Phys. Lett. 88 (2006), 232902.
[26] W. Ma, L.E. Cross, Flexoelectric effect in ceramic lead zirconate titanate, Appl. Phys. Lett. 86 (2005), 072905.
[27] L. Shu, X. Wei, L. Jin, Y. Li, H. Wang, X. Yao, Enhanced direct flexoelectricity in paraelectric phase of $Ba(Ti_{0.87}Sn_{0.13})O_3$ ceramics, Appl. Phys. Lett. 102 (2013), 152904.
[28] A. Abdollahi, F. Vasquez-Sancho, G. Catalan, Piezoelectric Mimicry of Flexoelectricity, Phys. Rev. Lett. 121 (2018), 205502.
[29] F. Li, M.J. Cabral, B. Xu, Z. Cheng, E.C. Dickey, J.M. LeBeau, J. Wang, J. Luo, S. Taylor, W. Hackenberger, L. Bellaiche, Z. Xu, L.-.Q. Chen, T.R. Shrout, S. Zhang, Giant piezoelectricity of Sm-doped $Pb(Mg_{1/3}Nb_{2/3})O_3$-$PbTiO_3$ single crystals, Science 364 (2019) 264–268.
[30] B. Chu, W. Zhu, N. Li, E. Cross, Flexure mode flexoelectric piezoelectric composites, J. Appl. Phys. 106 (2009), 104109.
[31] Y. Li, L. Shu, W. Huang, X. Jiang, H. Wang, Giant flexoelectricity in $Ba_{0.6}Sr_{0.4}TiO_3$/$Ni_{0.8}Zn_{0.2}Fe_2O_4$ composite, Appl. Phys. Lett. 105 (2014), 162906.
[32] S. Huang, H.-.M. Yau, H. Yu, L. Qi, F. So, J.-.Y. Dai, X. Jiang, Flexoelectricity in a metal/ferroelectric/semiconductor heterostructure, AIP Adv 8 (2018), 065321.
[33] C. Li, Z. Wang, F. Li, Z. Rao, Z. Huang, W. Huang, Z. Shen, S. Ke, L. Shu, Large flexoelectric response in PMN-PT ceramics through composition design, Appl. Phys. Lett. 115 (2019), 142901.
[34] J. Narvaez, F. Vasquez-Sancho, G. Catalan, Enhanced flexoelectric-like response in oxide semiconductors, Nature 538 (2016) 219.
[35] X. Wen, D. Li, K. Tan, Q. Deng, S.Flexoelectret Shen, An electret with a tunable flexoelectric like response, Phys. Rev. Lett. 122 (2019), 148001.
[36] L. Shu, S. Ke, L. Fei, W. Huang, Z. Wang, L. Gong, X. Jiang, L. Wang, F. Li, S. Lei, Z. Rao, Y. Zhou, R. Zheng, X. Yao, Y. Wang, M. Stengel, G. Catalan, Photoflexoelectric effect in halide perovskites, Nat. Mater. 19 (2020) 605.
[37] X. Zhang, Q. Pan, D. Tian, W. Zhou, P. Chen, H. Zhang, B Chu, Large flexoelectriclike response from the spontaneously polarized surfaces in ferroelectric ceramics, Phys. Rev. Lett. 121 (2018), 057602.
[38] S. Huang, T. Kim, D. Hou, D. Cahn, J.L. Jones, X. Jiang, Flexoelectric characterization of $BaTiO_3$-0.08$Bi(Zn_{1/2}Ti_{1/2})O_3$, Appl. Phys. Lett. 110 (2017), 222904.
[39] L. Shu, M. Wang, X. Jiang, F. Li, N. Zhou, W. Huang, T Wang, Frequency dispersion of flexoelectricity in PMN-PT single crystal, AIP Adv 7 (2017), 015010.
[40] B. Wang, Y. Gu, S. Zhang, L.-.Q. Chen, Flexoelectricity in solids: progress, challenges, and perspectives, Prog. Mater. Sci. 106 (2019), 100570.
[41] L. Shu, R. Liang, Z. Rao, Flexoelectric materials and their related applications: a focused review, J. Adv. Ceram. 8 (2019) 153.
[42] A. Biancoli, C.M. Fancher, J.L. Jones, D. Damjanovic, Breaking of macroscopic centric symmetry in paraelectric phases of ferroelectric materials and implications for flexoelectricity, Nature Mater 14 (2015) 224.
[43] L.M. Garten, S. Trolier-Mckinstry, Enhanced flexoelectricity through residual ferroelectricity in barium strontium titanate, J Appl Phys 117 (2015), 094102.
[44] J. Narvaez, G. Catalan, Origin of the enhanced flexoelectricity of relaxor ferroelectrics, Appl. Phys. Lett. 104 (2014), 162903.
[45] J. Narvaez, S. Saremi, J. Hong, M. Stengel, G. Catalan, Large flexoelectric anisotropy in paraelectric barium titanate, Phys. Rev. Lett. 115 (2015), 037601.
[46] T. Maiti, R. Guo, A.S. Bhalla, Structure-Property Phase Diagram of $BaZr_xTi_{1-x}O_3$ System, J. Am. Ceram. Soc. 91 (2008) 1769.
[47] L. Zhao, X. Ke, W. Wang, M. Fang, A. Xiao, L. He, L.Gao Zhang, J. Wang, Y. Ren, X. Mechanism of electrostrain enhancement in the single rhombohedral phase region of Ba $(Ti_{1-x}Zr_x)$ O_3 ceramics, J. Alloy Compd. 788 (2019) 748.

[48] X. Ke, S. Yang, Y. Wang, D. Wang, L. Zhao, J. Gao, Y. Wang, X Ren, Existence of a Quadruple Point in Binary Ferroelectric Phase Diagrams, Phys. Rev. B 103 (2021), 085132.
[49] R. Ahluwalia, A.K. Tagantsev, P. Yudin, N. Setter, N. Ng, D.J. Srolovitz, Influence of flexoelectric coupling on domain patterns in ferroelectrics, Phys. Rev. B 89 (2014), 174105.
[50] Y. Gu, Z. Hong, J. Britson, L.-.Q. Chen, Nanoscale mechanical switching of ferroelectric polarization via flexoelectricity, Appl. Phys. Lett. 106 (2015), 022904.
[51] P.V. Yudin, R. Ahluwalia, A.K. Tagantsev, Upper bounds for flexoelectric coefficients in ferroelectrics, Appl. Phys. Lett. 104 (2014), 082913.
[52] P. Yudin, J. Duchon, O. Pacherova, M. Klementova, T. Kocourek, A. Dejneka, M. Tyunina, Ferroelectric phase transitions induced by a strain gradient, Phys. Rev. Res. 3 (2021), 033213.
[53] Z. Hong, X. Ke, D. Wang, S. Yang, X. Ren, Y. Wang, Role of point defects in the formation of relaxor ferroelectrics, Acta Mater 225 (2022), 117558.
[54] S.-.E. Park, T.R. Shrout, Ultrahigh strain and piezoelectric behavior in relaxor based ferroelectric single crystals, J. Appl. Phys. 82 (1997) 1804.
[55] J. Kelly, M. Leonard, C. Tantigate, A. Safari, Effect of composition on the electromechanical properties of (1-x)Pb($Mg_{1/3}Nb_{2/3}$)O_3-$x$$PbTiO_3$ ceramics, J. Am. Ceram. Soc. 80 (1997) 957.
[56] J. Li, D. Zhang, S. Qin, T. Li, M. Wu, D. Wang, Y. Bai, X. Lou, Large room-temperature electrocaloric effect in lead-free $BaHf_xTi_{1-x}O_3$ ceramics under low electric field, Acta Mater. 115 (2016) 58.
[57] J. Iniguez, S. Ivantchev, J.M. Perez-Mato, A Garcia, Devonshire-Landau free energy of BaTiO3 from first principles, Phys. Rev. B 63 (2001), 144103.
[58] R. Yuan, Z. Liu, P.V. Balachandran, D. Xue, Y. Zhou, X. Ding, J. Sun, D. Xue, T. Lookman, Accelerated discovery of large electrostrains in $BaTiO_3$-based piezoelectrics using active learning, Adv. Mater. 30 (2018), 1702884.